Sensors and Materials, Vol. 28, No. 7 (2016) 777–784
MYU Tokyo

S & M 1237

Amperometric Nitrite-Ion Sensor Based on Electrodeposited Sm-Based Perovskite-Type Oxide Thick-Film Electrode

Takahiro Yatsunami, Satoko Takase, and Youichi Shimizu*

Department of Applied Chemistry, Kyushu Institute of Technology,
1-1 Sensui-cho, Tobata, City of Kitakyushu, Fukuoka 804-8550, Japan

(Received September 30, 2015; accepted March 7, 2016)

Keywords: perovskite-type oxide, nitrite-ion sensor, carbon-felt electrodes, amperometric, electrophoretic deposition

Perovskite-type oxide Sm*B*O_3 (*B* = Cr, Mn, Fe, Co) powders were prepared by a polymer precursor method at 750 °C and systematically investigated for electrochemical sensing properties for NO_2^-. The Sm*B*O_3-modified carbon-felt electrodes could be prepared by an electrophoretic deposition (EPD) method without sintering. Among the oxide deposited electrodes, the $SmFeO_3$ modified electrode showed the highest sensitivity to NO_2^- with 11.9 mA M^{-1} cm^{-2} and a linear sensing range between 5.0×10^{-5} and 1.0×10^{-3} M at +0.85 V vs Ag / AgCl with high selectivity for NO_2^- and no response to most other anions. A good correlation was observed between electrochemical activity toward nitrite-ion oxidation and oxygen adsorption properties of the oxides.

1. Introduction

It is known that nitrite ion (NO_2^-) reacts easily with proteins to produce carcinogenic N-nitrosamines which cause esophageal cancer and methemoglobinemia *in vivo*. Although it is used as an antioxidant for foods and beverages, nitrite ion itself is high toxic, and it should be at a concentration less than 65 μM in drinking water according to the standards of the World Health Organization (WHO). It is also well known that NO_2^- causes eutrophication in closed water systems. Thus, quantitative analysis of NO_2^- has become very important. Thus far, nitrite ion is typically analyzed by a spectrophotometric method[1,2] or by ion chromatography, but these methods are complicated and not suitable for on-site monitoring. In contrast, electrochemical methods have aroused considerable interest as possibilities for the design of compact and low-cost ion sensors. As electrochemical NO_2^- sensing materials, various metal complexes[3,4] as ionophores for potentiometric sensors, and carbon nanomaterials,[5,6] metal nanomaterials,[7–12] metal organic complexes,[13,14] and conducting polymers[15] for amperometric sensors have been reported. Oxide-based NO_2^- sensing materials, such as hollow Fe_2O_3 nano-polyhedrons,[16] Fe_2O_3 nanoparticle-decorated reduced graphene oxide nanosheets,[17] and nanoporous Fe_2O_3-CoO composites[18] have been developed. These sensors revealed a remarkable interaction between elemental iron and NO_2^-. These results indicated that iron-based mixed oxides might be suitable candidate materials

*Corresponding author: e-mail: shimizu.youichi366@mail.kyutech.jp

ISSN 0914-4935

for NO_2^- sensing. We have proposed various electrochemical ion sensors for the hydrogen phosphate ion[19] and hydrogen peroxide[20] based on the considerable electrocatalytic properties of perovskite-type oxides. It has also been reported that Sm-based perovskite-type oxides showed high sensing abilities among the lanthanoids (La, Nd, Sm, Gd, and Dy).[21,22] In this study, we have systematically evaluated electrochemical catalytic activities of perovskite-type oxide SmBO$_3$ (B = Cr, Mn, Fe, Co)-modified carbon-felt electrodes prepared by electrophoretic deposition (EPD) for amperometric NO_2^- sensing. The $SmFeO_3$ modified carbon-felt electrode showed the highest NO_2^- sensing properties; these properties were related to the amount and the strength of adsorbed oxygen on the surface of the $SmFeO_3$.

2. Experimental

2.1 Preparation of perovskite-type oxide powders

Perovskite-type oxide SmBO$_3$ powders were prepared by a polymer precursor method.[23,24] A 10 mmol quantity of metal (Sm, Cr, Mn, Fe, Co) nitrate of reagent grade was dissolved in 50 mL of ethylene glycol (EG), which was mixed with 40 mmol of acetylacetone (AcAc) as a coordinating agent and 7.5 wt% polyethylene glycol (PEG: MW 200) as a polymer additive, until a viscous sol was formed. These polymer precursor solutions were dried in ambient air to form xerogel powders, which were then heat-treated at 750 °C for 2 h. The crystal structures of the powders obtained were elucidated by X-ray diffraction (XRD) analysis using CuKα radiation (λ = 0.15405 nm) (X-ray diffraction spectroscopy, Ultima IV, Rigaku Ltd.). The specific surface area (SSA) of the powders was determined by Brunauer, Emmett, and Teller (BET) method from nitrogen adsorption isotherms obtained at 77 K using an automatic specific surface area analyzer (BELLSORP-mini-II, MicrotracBEL Ltd.). Chemical states of metals and oxide on the surface of the oxide powders were characterized by X-ray photoelectron spectroscopy (XPS) (AXIS-Nova, Shimadzu Kratos Ltd.) using an Al Kα source, in which the binding energies were calibrated using the C_{1s} line at 284.6 eV. Temperature programmed desorption (TPD) experiments were carried out using a catalyst analyzer (BELCAT-B-SPS, MicrotracBEL Ltd.) as follows. Each sample was evacuated for 15 min at 750 °C, then exposed to 50 mL/min of oxygen for 1 min at the same temperature, and cooled to 50 °C in the same atmosphere. After the evacuation, the sample was heated at a rate of 10 °C/min in a helium stream (30 mL/min), and desorbed oxygen was monitored by a thermal conducting detector.

2.2 Preparation of perovskite-type oxide thick films by EPD

SmBO$_3$ modified carbon-felt (SmBO$_3$/CF) electrodes were prepared by EPD.[25] A 0.24 g sample of each oxide powder was suspended in 50 mL AcAc and mixed in a planetary ball mill (L-P1, Ito Seisakusho Co., Ltd.) at 250 rpm for 30 min. After the ball-mill treatment, 25 mg I_2 and 50 mL AcAc were added to make an EPD electrolyte solution. EPD was carried out using carbon felt (CF; GF-20-2F, Nippon carbon Ltd.) as a working electrode and a Pt plate as a counter electrode. The distance between the two electrodes was fixed at 10 mm. After ultrasonic wave treatment of the EPD electrolyte solution for 30 min, EPD was performed by applying a constant DC voltage at −50 V vs the Pt electrode for 10 min at room temperature. The SmBO$_3$/CF electrodes were washed with ethanol and dried at 100 °C. Further sintering of the electrodes was not carried out.

2.3 Electrochemical measurements

Cyclic voltammetry and amperometric measurements were performed using an electrochemical analyzer (model 1140A, ALS Ltd.) using a Pt plate and an Ag/AgCl (KCl sat.) as the counter and a reference electrodes, respectively. Figure 1 shows a diagram of the sensor electrode using oxide modified carbon felt. All electrochemical experiments were carried out in 50 mL pH 7.0 Tris-HCl buffer solution at 30 °C after oxygen or nitrogen bubbling for 30 min. Amperometric sensing properties were measurement by a batch method using solutions of reagent grade $NaNO_2$ or other sodium salts ($NaNO_3$, Na_2SO_4, Na_2HPO_4, $NaHCO_3$, CH_3COONa, and NaSCN) added dropwise to the analyte solution with a micropipette to control the ion concentrations.

3. Results and Discussion

3.1 Characterization of the oxide powders

Figure 2 shows the XRD patterns of SmBO$_3$ (B = Cr, Mn, Fe, Co) powders prepared at 750 °C for 2 h by the polymer precursor method. The powders consisted of primarily single-phase perovskite-type oxide. The SSAs of $SmCrO_3$, $SmMnO_3$, $SmFeO_3$, and $SmCoO_3$ were between 1.9 and 8.6 $m^2\ g^{-1}$ as shown in Table 1. SEM images of these powders are shown in Fig. 3. $SmCrO_3$ and $SmCoO_3$ powders were partially sintered and formed large particles as shown by their smaller SSAs. Although $SmMnO_3$ powder consisted of small particles less than 50 nm in diameter, these particles aggregated partially to form larger particles. Among them, $SmFeO_3$ powder consisted of relatively small particles of ca. 90 nm in diameter.

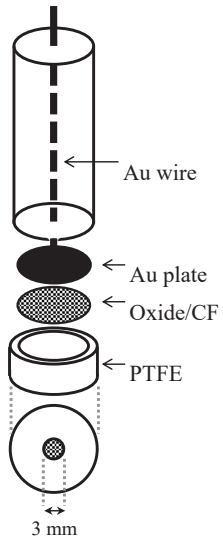

Fig. 1. Schematic diagram of sensor electrode with oxide modified carbon felt.

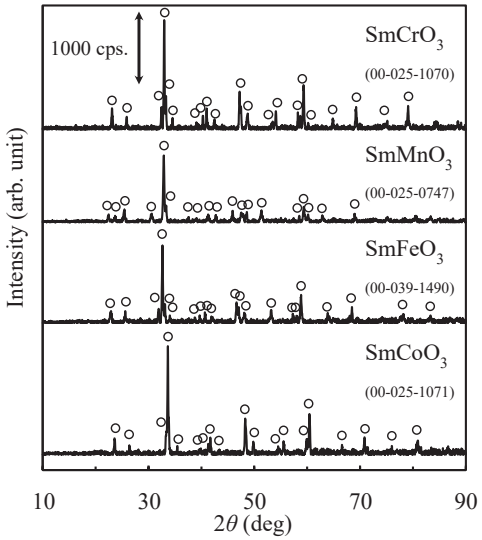

Fig. 2. XRD patterns of SmBO$_3$ powders (B = Cr, Mn, Fe, Co) prepared at 750 °C for 2 h (Numbers in the figure are the ICDD numbers of the International Center for Diffraction Data).

Table 1
BET surface areas, sensor performance for NO_2^-, and surface oxygen states of SmBO$_3$ (B = Cr, Mn, Fe, Co) powders.

	$SmCrO_3$	$SmMnO_3$	$SmFeO_3$	$SmCoO_3$	Fe_2O_3
BET S.A. ($m^2\ g^{-1}$)	5.0	8.6	8.3	1.9	–
Sensitivity* (mA M^{-1} cm^{-2})	9.9	4.3	11.9	9.4	4.5
Linear range (μM)	200–1000	200–900	50–1000	100–800	100–1000
O_A / (O_A + O_L) (%)**	43.5	36.8	46.3	44.0	14.7

*at +0.85 V vs Ag/AgCl.

**O_A: amount of adsorbed oxygen, O_L: amount of lattice oxygen.

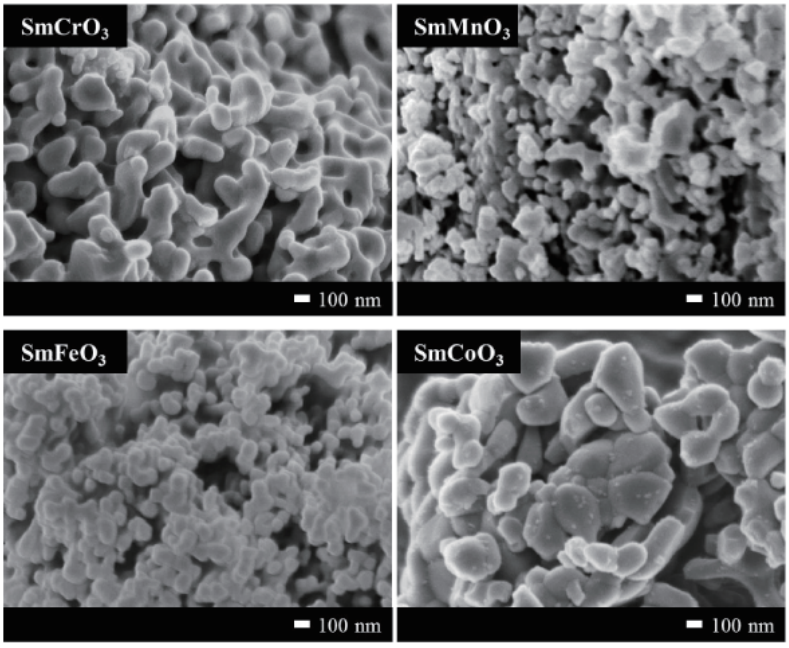

Fig. 3. SEM images of SmBO$_3$ (B = Cr, Mn, Fe, Co) powders.

3.2 Electrochemical measurements

Figure 4 shows cyclic voltammograms of the SmBO$_3$/CF (B = Cr, Mn, Fe, Co) electrodes in aqueous solutions at various NO_2^- concentrations with oxygen bubbling. The cyclic voltammograms in $SmCrO_3$, $SmMnO_3$, and $SmCoO_3$ systems showed an increase in anodic current depending on NO_2^-concentration; however, they still had large hysteresis even in a buffer solution. The hysteresis in $SmCrO_3$, $SmMnO_3$, and $SmCoO_3$ systems should be primarily due to the redox of transition metals (Cr, Mn, Co) in the perovskite-type oxides. However, the anodic current of the SmFeO3/CF electrode around +0.85 V vs Ag/AgCl increased simply with increasing NO_2^- concentration.

Figure 5 shows a typical transient response curve of the $SmFeO_3$/CF electrode to various concentration of NO_2^- at +0.85 V vs Ag/AgCl. The anodic current of the $SmFeO_3$/CF electrode increased with increasing NO_2^- concentration. The 90% response time from 100 to 200 μM was about 3 min. The dependence of response current on NO_2^- concentration of the $SmFeO_3$/CF electrode under O_2 and N_2 bubbling is shown in Fig. 6. Response currents increased with increasing NO_2^- concentration with O_2 and N_2 bubbling. The response current under O_2 bubbling was slightly larger than that with N_2, especially in the lower concentration range. The $SmFeO_3$/CF electrode

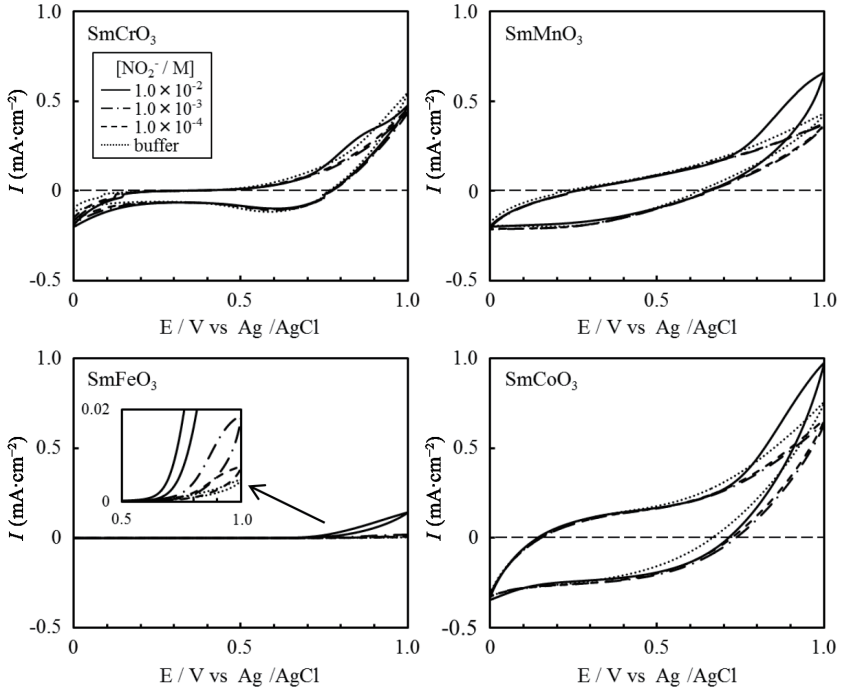

Fig. 4. Cyclic voltammograms of SmBO$_3$/CF electrodes for various NO_2^- concentrations (Scan rate: 10 mV/s).

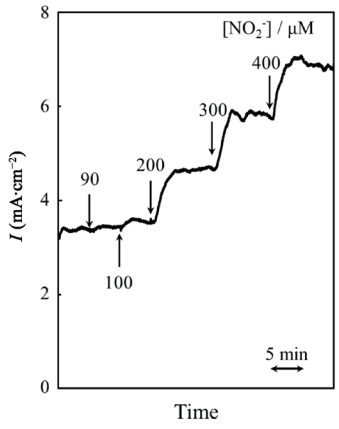

Fig. 5. Response transient curve of the $SmFeO_3$/CF electrode to NO_2^- (+0.85 V vs Ag/AgCl).

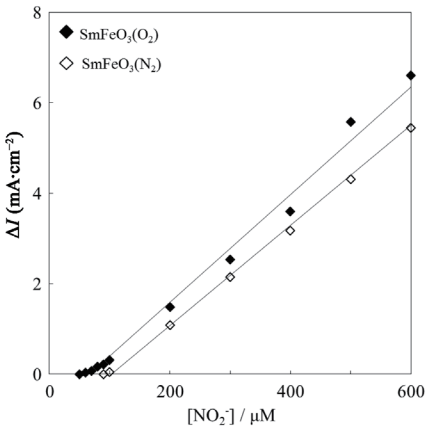

Fig. 6. Dependence of response current on NO_2^- concentration of the $SmFeO_3$/CF electrode with O_2 or N_2 bubbling (+0.85 V vs Ag/AgCl).

showed a linear sensitivity between 5.0×10^{-5} and 6.0×10^{-3} M with a sensitivity of 11.9 mA M^{-1} cm^{-2} under O_2 bubbling. This may be related to the reaction with the adsorbed oxygen as described in the following. Hereafter, all response characteristics were measured with O_2 bubbling. Figure 7 shows response characteristics of the SmBO$_3$/CF (B = Cr, Mn, Fe, Co) and Fe_2O_3/CF electrodes. The NO_2^- sensitivity for the SmBO$_3$/CF systems was in the order $SmFeO_3$ > $SmCrO_3$ > $SmCoO_3$ > $SmMnO_3$ = Fe_2O_3, as summarized in Table 1. This means that the $SmFeO_3$ perovskite-type structure plays an important role in electrochemical oxidation of NO_2^- ion. These results also indicated that the Fe surface in the oxides might be the active site for the reaction with NO_2^-; Fe in $SmFeO_3$ has higher surface activity for NO_2^- than Fe in Fe_2O_3.

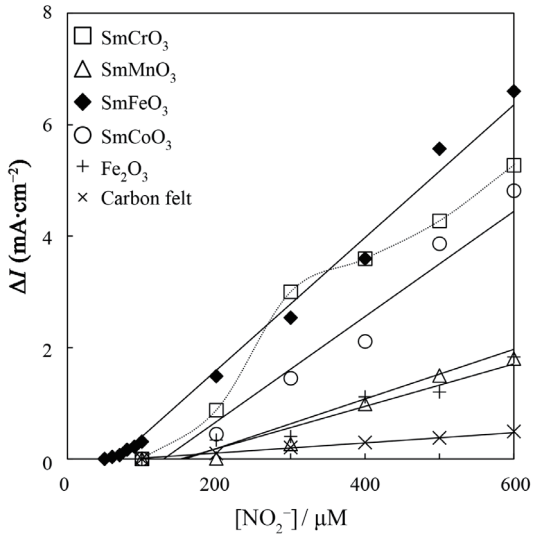

Fig. 7. Dependence of response current on NO_2^- concentration for various electrodes with O_2 bubbling (+0.85 V vs Ag/AgCl).

The $SmFeO_3$/CF electrode showed no significant amperometric response at +0.85 V vs Ag/AgCl for NO_3^-, SO_4^{2-}, HPO_4^{2-}, CH_3COO^-, HCO_3^-, and SCN^- anions between 10 and 1000 μM. Thus, the $SmFeO_3$/CF electrode exhibited high selectivity for NO_2^-.

3.3 Sensing mechanism

To investigate the sensing mechanism, surface chemical analysis was carried out by XPS and TPD. First, XPS spectra at O_{1s} of Sm*B*O_3 (*B* = Cr, Mn, Fe, Co) powders were recorded as shown in Fig. 8. Lower and higher binding energy (BE) peaks were identified as lattice oxide (O_L) and adsorbed oxygen (O_A), respectively.[26] The O_A / (O_A + O_L) ratio on the surface of $SmFeO_3$ was the highest among the Sm*B*O_3 systems as shown in Table 1. Figure 9 compares XPS spectra between Fe_2O_3 and $SmFeO_3$ at O_{1s} and Fe_{2p}. The amount of adsorbed oxygen on Fe_2O_3 was very small compared with that on $SmFeO_3$. The BE of lattice oxygen in Fe_2O_3 was relatively large as shown in Fig. 9 (a); thus, Fe_2O_3 crystals are characterized by strong metal-oxygen bonding. Oxidation states of Fe in Fe_2O_3 and $SmFeO_3$, included Fe^{2+}, Fe^{3+}, and Fe^{4+} as shown in Fig. 9(b). The presence of Fe^{2+}, especially in $SmFeO_3$, should allow the high valence of Fe^{4+} and/or oxygen vacancies in the oxide.

To investigate the oxygen adsorption-desorption properties of perovskite-type oxides, TPD profiles of the Sm*B*O_3 (*B* = Cr, Mn, Fe, Co) powders were determined. As shown in Fig. 10, two peaks appear at around 250 °C and over 450 °C in the TPD profiles of the Sm*B*O_3 (*B* = Cr, Mn, Fe, Co) powders. The former and latter peaks seem to be chemically bonded surface oxygen and lattice oxygen, respectively.[27,28] Oxygen desorption of chemically bonded surface oxygen from the $SmFeO_3$ was noted from ca. 240 °C, which was the lowest observed temperature for the Sm*B*O_3 (*B* = Cr, Mn, Fe, Co) series. From these TPD and XPS measurements, the surface of the $SmFeO_3$ has the most active oxygen species among the oxides.

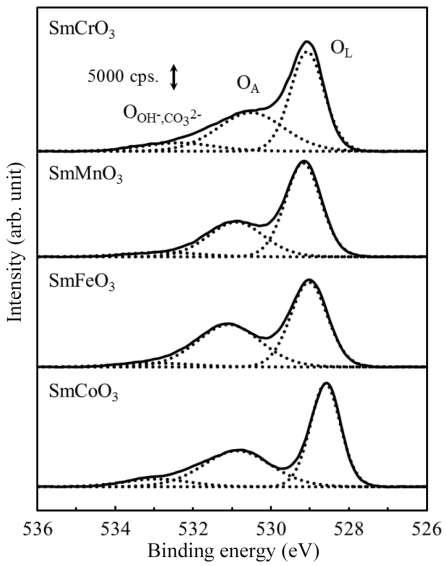

Fig. 8. XPS spectra of O_{1s} of SmBO$_3$ (B = Cr, Mn, Fe, Co) powders.

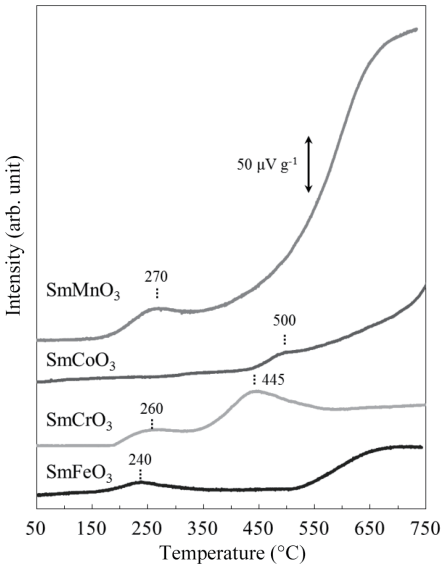

Fig. 10. O_2-TPD profiles of SmBO$_3$ (B = Cr, Mn, Fe, Co) powders.

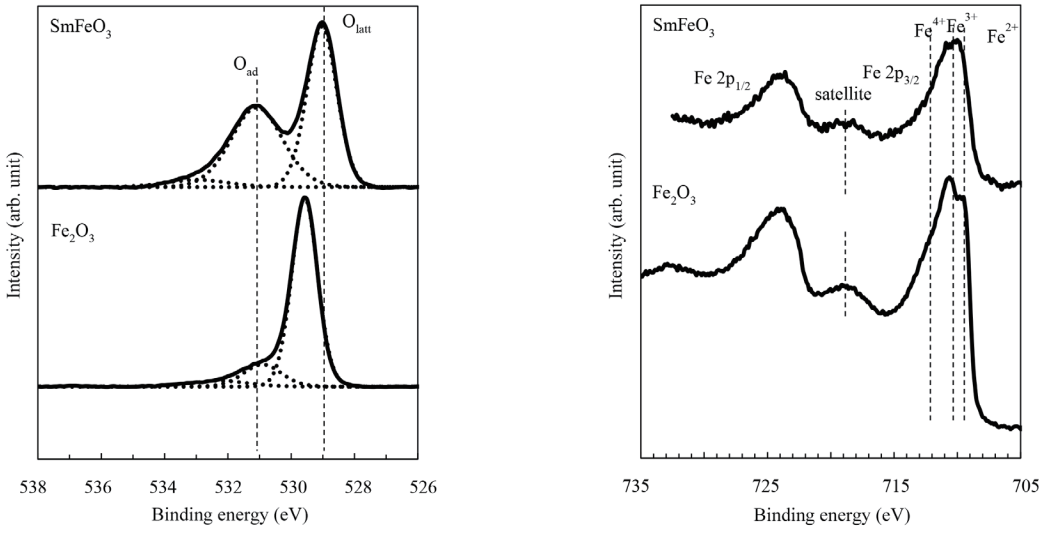

Fig. 9. XPS spectra of (a) O_{1s} and (b) Fe_{2p} of $SmFeO_3$ and Fe_2O_3 powders.

From these results, the sensing mechanism may be expressed as Eqs. (1) and (2):

$$SmFeO_3\text{-}O_{ad}^- + H_2O \rightarrow SmFeO_3\text{-}2OH_{ad}^- \quad (1)$$

$$SmFeO_3\text{-}2OH_{ad}^- + SmFeO_3NO_2^- \rightarrow SmFeO_3 + NO_3^- + 2e^- + H_2O \quad (2)$$

A possible reaction responsible for NO_2^- response was proposed to be the oxidation reaction of NO_2^- by adsorbed OH_{ad}^- on a Fe site in $SmFeO_3$. The electrtocatalytic activity for NO_2^- oxidation

is thought to be influenced by the presence of OH_{ad}^- on the oxide surface which was formed by the reaction between O_{ad}^- and H_2O. In these results, the $SmFeO_3$/CF electrode showed higher sensitivity than the Fe_2O_3/CF or other electrodes.

4. Conclusions

The Sm*B*O_3 (*B* = Cr, Mn, Fe, Co) powders could be prepared by a polymer precursor method at 750 °C. The Sm*B*O_3-modified CF electrodes were fabricated by an EPD method without sintering. Among the oxides tested, the $SmFeO_3$/CF electrode showed the highest NO_2^- sensitivity, 11.9 mA M^{-1} cm^{-2}, and a wide linear response range between 5.0×10^{-5} and 1.0×10^{-3} M. Furthermore, the $SmFeO_3$/carbon electrode showed no response to NO_3^-, SO_4^{2-}, HPO_4^{2-}, CH_3COO^-, HCO_3^-, and SCN^- up to 1000 μM. The high NO_2^- sensitivity of $SmFeO_3$ arises from the large amount of adsorbed oxygen, which should strongly correlate to the electrocatalytic activity of NO_2^- oxidation.

Acknowledgements

The authors are grateful to the Center for Instrumental Analysis, Kyushu Institute of Technology, for the XPS measurements.

References

1 V. V. Kumar and S. P. Anthony: Anal. Chim. Acta **57** (2014) 842.
2 T. Zhang, H. Fan, and Q. Jin: Talanta **81** (2010) 95.
3 M. Pietrzak and M. E. Meyerhoff: Anal. Chem. **81** (2009) 3637.
4 B. Néel, M. G. Asfhar, G. A. Crespo, M. Pawlak, D. Dorokhin, and E. Bakker: Electroanalysis **26** (2014) 473.
5 M. Eguílaz, L. Agüí, P. Yáñez-Sedeño, and J. M. Pingarrón: J. Electroanal. Chem. **644** (2010) 30.
6 D. Ye, L. Luo, Y. P. Ding, Q. Chen, and X. Liu: Analyst **136** (2011) 4563.
7 S. Yang, X. Zeng, X. Liu, W. Wei, S. Luo, Y. Liu, and Y. Liu: J. Electroanal. Chem. **639** (2010) 181.
8 Y. Zhang, Y. Zhao, S. Yuan, H. Wang, and C. He: Sens. Actuators, B **185** (2013) 602.
9 N. Wang, X. Cao, X. Cai, Y. Xu, and L. Guo: Analyst **135** (2010) 2106.
10 M. Pal and V. Ganesan: Analyst **135** (2010) 2711.
11 H. Mao, X. Liu, D. Chao, L. Cui, Y. Li, W. Zhang, and C. Wang: J. Mater. Chem. **20** (2010) 10277.
12 S. Gupta and R. Prakash: RSC Advances **4** (2014) 7521.
13 C. A. Caro, F. Bedioui, and J. H. Zagal: Electrochim. Acta **47** (2002) 1489.
14 C. Wang, R. Yuan, Y. Chai, S. Chen, Y. Zhang, F. Hu, and M. Zhang: Electrochim. Acta **62** (2012) 109.
15 Y. H. Cheng, C. W. Kung, L. Y. Chou, R. Vittal, and K. C. Ho: Sens. Actuators, B **192** (2014) 762.
16 X. Cao, Y. Xu, and N. Wang: Electrochim. Acta **59** (2012) 81.
17 S. Radhakrishnan, K. Krishnamoorthy, C. Sekar, J. Wilson, and S. J. Kim: Appl. Catal., B **22** (2014) 148.
18 J. Wang, D. Zhao, Y. Zhang, J. Li, and C. Xu: Anal. Methods **6** (2014) 3147.
19 S. Takase, T. Matsumoto, and Y. Shimizu: Electrochemistry **78** (2010) 150.
20 S. Takase, A. Ishikawa, and Y. Shimizu: Electrochemistry **69** (2001) 272.
21 H. Aono, E. Traversa, M. Sakamoto, and Y. Sadaoka: Sens. Actuators, B **94** (2003) 132.
22 T. Tasaki, S. Takse, and Y. Shimizu: Sens. Actuators, B **187** (2013) 128.
23 T. Iseri, M. Kawasaki, S. Takase, and Y. Shimizu: ITE Lett. Batteries New Technol. Med. **5** (2006) 231.
24 Y. Shimizu and T. Murata: J. Am. Ceram. Soc. **80** (1997) 2702.
25 S. Y. Ng and A. R. Boccaccini: Mater. Sci. Eng., B **116** (2005) 208.
26 M. Mori, Y. Iwamoto, M. Asamoto, Y. Itagaki, H. Yahiro, Y. Sadaoka, S. Takase, Y. Shimizu, M. Yuasa, K. Shimanoe, H. Kusaba, and Y. Teraoka: Catal. Today **139** (2008) 125.
27 Y. Teraoka, M. Yoshimatsu, N. Yamazoe, and T. Seiyama: Chem. Lett. **6** (1984) 893.
28 H. M. Xhang, Y. Shimizu, Y. Teraoka, N. Miura, and N. Yamazoe: J. Catal. **121** (1990) 432.